International Journal of Mechanical Sciences 251 (2023) 108325

Contents lists available at ScienceDirect

International Journal of Mechanical Sciences

journal homepage: www.elsevier.com/locate/ijmecsci

# Layer jamming: Modeling and experimental validation

Fabio Caruso *, Giacomo Mantriota, Vincenzo Moramarco, Giulio Reina

*Department of Mechanics, Mathematics and Management, Polytechnic University of Bari, Via E. Orabona 4, 70125, Bari, Italy*

ARTICLE INFO

*Keywords:*
Layer jamming
Theoretical model
Variable stiffness
Experimental validation
Soft robotics
Vacuum jamming

ABSTRACT

The ability to control and tune the stiffness of soft structures is one of the most important challenges in soft robotics. This is crucial in applications that require both compliance and the ability to withstand high forces. Among the various techniques, layer jamming represents a promising solution. Despite the increasing interest, the existing analytical models are not able to describe the behavior of these structures beyond the initial deformation phase. In this work, we propose an analytical model that predicts the behavior of these structures in all deformation phases, overcoming the limitations of existing models. Our previous approach is extended by explicitly taking into account the increase in stiffness due to the overhangs of the structure outside the constraining supports. We conduct experimental tests and finite element simulations to validate the predictions of the proposed model. The experimental and finite element results are in good agreement with theoretical predictions, especially considering that no fitting parameters have been used. Additionally, we analyze the effect of the main design parameters, including the number of layers, vacuum pressure and coefficient of friction, as well as the energy dissipated by friction during a load–unload cycle. We believe that this work represents a significant step forward in understanding the complex mechanisms underlying the mechanics of layer jamming structures that could be useful in helping researchers design more advanced variable stiffness applications in soft robotics.

## 1. Introduction

In the last two decades, researchers started to design robots using compliant materials giving life to a new exciting field called "soft robotics" [1–3]. This shift came from the desire to overcome the limitations of hard robots to safely interact with humans and to adapt autonomously to unstructured environments [4–6]. However, building robots with soft materials led to new and interesting challenges [7–9].

One of them is the ability to control and tune the stiffness of the soft structures [10–12]. This is particularly important in applications that require both compliance and the ability to withstand high forces, such as minimally invasive surgery [13–15], wearable haptics [16,17], soft grippers [18–21] and smart fabrics [22–24]. Depending on the specific application, researchers came up with different techniques to achieve stiffness modulation, including thermal [25,26], magnetic [27], electric [28] and pressure-induced (jamming [29]) stimulation. Among these techniques, jamming-based systems are usually preferred for their easy fabrication process and fast and reversible transition between soft and rigid states with very limited volume variation.

The jamming phenomenon generally consists of granules [30,31], fibers [32–35] or layers [36,37] confined in a thin airtight membrane connected to a vacuum source. When vacuum is introduced inside the membrane frictional coupling increases, resulting in a dramatic change in stiffness. This simple yet effective technique has proven to be useful in several applications.

In their pioneering work, Brown and colleagues [38] used granular jamming to develop a universal soft gripper able to pick up unfamiliar objects of widely varying shape and surface properties. In a subsequent work [39] the same authors demonstrated that introducing both positive and negative pressure improved gripper's speed, error tolerance and placement accuracy. Using the same concept, Licht et al. [40] demonstrated that granular jamming grippers can also be used for grasping tasks in deep-sea environments with ambient pressures exceeding 100 atmospheres. As a variable stiffness element, granular jamming has been also used in medical applications. Ranzani et al. [41] exploited granular jamming to achieve stiffness change in a bioinspired soft endoscope. In a similar work, Cavallo et al. [42] introduced granular jamming in a soft retraction system to ensure both safe introduction and stable retraction into the abdominal cavity.

Although granular jamming has the advantage to easily conform to complex shapes, it requires a large volume of granular materials to provide enough stiffness when jammed. Mathematical models based on continuum theories [43–45], discrete element methods [46,47] and statistical mechanics [48,49] have been proposed to study the behavior

* Corresponding author.
*E-mail address:* fabio.caruso@poliba.it (F. Caruso).

https://doi.org/10.1016/j.ijmecsci.2023.108325
Received 20 December 2022; Received in revised form 8 March 2023; Accepted 16 March 2023
Available online 21 March 2023

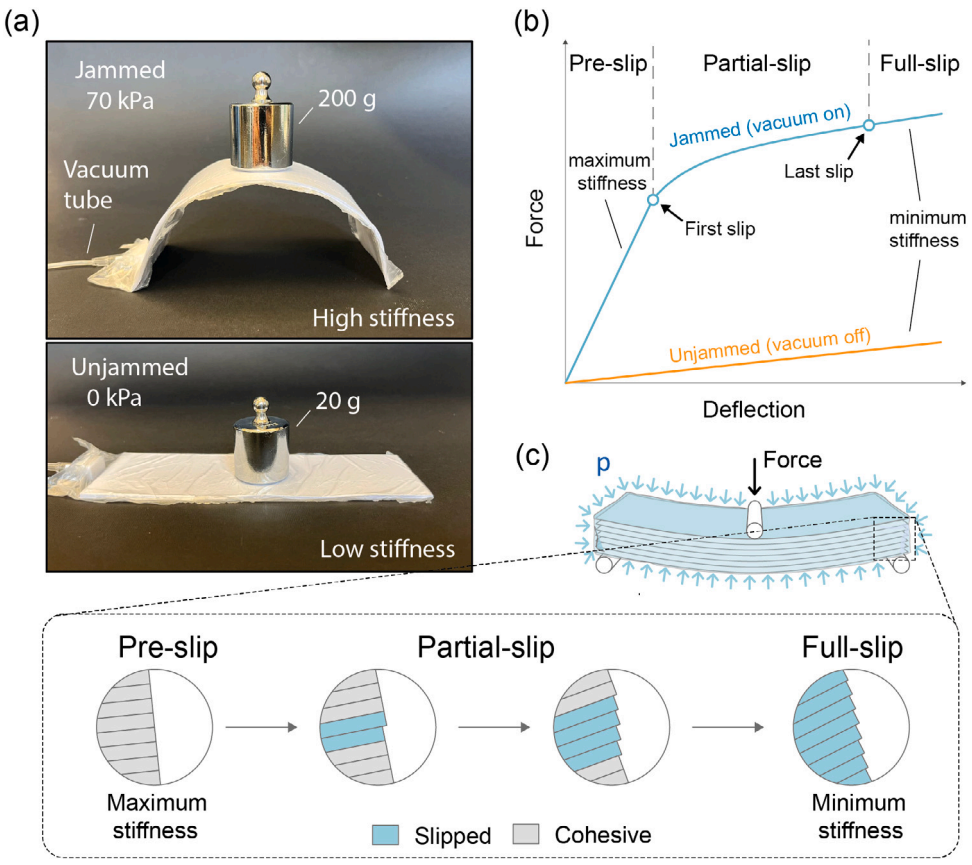


**Fig. 1.** Stiffness change and slip propagation in layer jamming systems. (a) Visualization of the dramatic change in stiffness when the structure is jammed (70 kPa) and unjammed (0 kPa). (b) Fundamental behavior of layer jamming structures subjected to three-point bending tests. (c) Schematic representation of slip propagation. In the pre-slip phase the shear stress at each interface remains below the static friction limit, the stiffness is maximum and the system behaves like a single beam. Then as the external load increases, the structure enters in the partial-slip phase. Here, slip starts from the central interface and propagates outward. The behavior becomes nonlinear and the stiffness decreases. In the last phase (Full-slip) all the layers are in slip and the stiffness is minimum.

of these systems, but they are often limited to circular particles and simple geometries, making them unfeasible to be used in real applications. In addition, conventional granular materials do not support tensile forces making them unsuitable in applications that require high bending stiffness [50].

To overcome these limitations researchers introduced the concept of layer jamming. Here, granules are replaced with thin flexible sheets resulting in a more compact design and the ability to withstand high bending moments. One of the first applications of this concept is represented by the snake-like manipulator developed by Kim et al. [51,52] in which thin layers are assembled into a helical pattern to maximize stiffness change between jammed and unjammed states. Ou et al.[53] introduced layer jamming to develop dynamic haptic interfaces with tunable-stiffness capabilities.

Inspired by these preliminary works, researchers started to explore the advantages of layer jamming in a wide variety of soft robotic applications. Several works employed layer jamming to increase the performance of soft grippers [54–56]. The low stiffness in the rest state allows the fingers to conform to the shape of the object being grasped, while the high stiffness upon activation ensures high holding forces [57–59]. Layer jamming has been also proposed in soft controllable dampers [60] and wearable orthosis [61,62]. Choi et al. [63] designed a soft wearable linear break in which the breaking force is controlled by the vacuum pressure applied to the layers.

Following the same principle, Narang et al. [64] demonstrated that layer jamming structures can be used to tune the impact response of aerial robots, while Wanasinghe et al. [65] integrated them in soft gloves as hand tremor suppressors.

Although the increasing interest, few studies tried to develop analytical models to understand the mechanical behavior of these structures. The mechanics of multi-layer structures is not new and has been extensively studied for predicting the behavior of laminate composites [66]. Analytical models [67] and numerical simulations [68] have been developed to predict both mechanical properties and interlaminar failure. However, these models are typically quite complex. They are based on higher order shear deformation theory to account for stresses at the interfaces caused by the variations of internal properties of the layers. While the complexity of these models is essential to accurately predict the behavior of laminate composites, they are overlay complex for layer jamming systems in which the behavior is simply controlled by friction and vacuum pressure.

Narang and colleagues [69] were the first to provide an analytical model, based on the Euler Bernoulli beam theory, to predict the change in stiffness due to slip propagation in a two-layer cantilever jamming structure subjected to a distributed load. In the same work [69] they developed finite element models to extend the predictions to many-layer jamming structures. These models were then validated with experiments showing excellent agreement. Subsequent research extended these models introducing a 3D FE-based numerical tool that predicts the mechanical response of layer jamming structures subjected to arbitrary loading and boundary conditions [70].

Although these works represent a significant step forward in the effort of understanding layer jamming systems, they have not yet provided analytical models for multi-layer jamming systems beyond the initial deformation phase. The main problem of finite element models is that the computational time increases with the number of layers. Therefore, for jamming structures with many layers, the computational

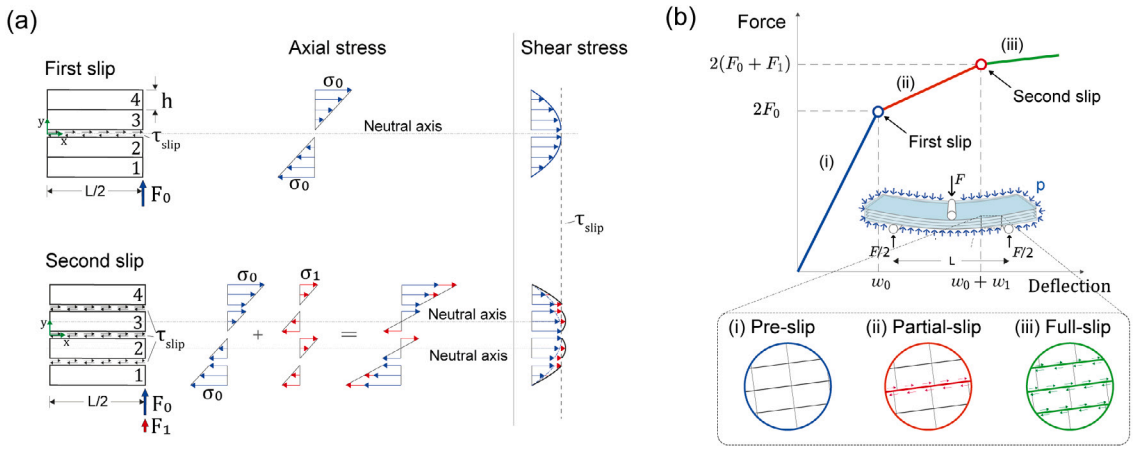


**Fig. 2.** Analytical model of four-layer jamming structures. (a) Schematic representation of the axial and shear stress distribution. When the transverse load is equal to $F_0$ the longitudinal shear stress at the central interface reaches the frictional limit ($\tau_{slip} = \mu p$) and layers 2 and 3 start to slip. As the external load is further increased by the additional load $F_1$, $\tau_{slip}$ is reached also at the interface between layers 1–2 and 3–4 and all the layers enter in slip. (b) Qualitative representation of the change in stiffness and slip propagation during a three-point bending test in all the three deformation phases.

time may become prohibitive and can significantly delay the design process.

To overcome this limitation, recently, we proposed for the first time an analytical model extended to a structure with an arbitrary number of layers [71]. We demonstrated that the typical nonlinear behavior of these structures can be well described with a piecewise linear approximation between subsequent slips. We also demonstrated how the slip propagates inside the structure and how these slips can be related to the gradual stiffness change (Fig. 1). Analytical predictions were compared with finite element simulations, both in a three-point bending and cantilever configuration [72], showing very good agreement.

In this work, we extended our previous model to take into account the phenomenon of curvature reversal caused by the overhanging portion of the structure outside the supports. This phenomenon has been observed both experimentally and with finite element simulations and causes an increase in bending stiffness. We also conducted experimental tests to validate theoretical predictions as well as finite element simulations to further validate the proposed approach. The model was able to predict with great accuracy the effect of the number of layers, vacuum pressure, friction coefficient, and energy dissipated by friction in a load–unload cycle, demonstrating that the complex intrinsic mechanics of these systems can be well approximated by a 2D analytical model.

The paper is organized as follows. In Section 2 we describe the derivation of the extended analytical model, highlighting the differences with respect to the model previously published by the authors. Section 3 describes the experimental details, while Section 4 presents the formulation of the finite element method used to validate the proposed model. The predictions of the model are compared with experiments and finite element simulations in Section 5. Finally, Section 6 concludes the article with the main findings and final considerations.

## 2. Analytical formulation

In this section, we extend our previously published analytical model [71], including the increase in stiffness due to the resistance to sliding of the overhanging portion of the structure outside the supports. This effect leads to curvature reversal, in which the structure shift from positive to negative curvature, an interesting phenomenon that has been shown both experimentally and with finite element simulations in the work of Narang et al. [69].

In order to facilitate the understanding of the model, in the following subsections we first derive the governing equations for a structure with only 4 layers and then we provide a general formulation that can be applied to a structure with an arbitrary number of layers.

### 2.1. Jamming structures with four layers

Consider a layer-jamming structure consisting of four layers subjected to a vacuum pressure $p$ while loaded in a three-point bending test. In the initial phase the shear stress at each interface is below the friction limit ($\mu p$) and the structure behaves like a single beam. As the external load increases, the structure will shift from the pre-slip to the partial-slip phase. The central interface is the first one that enters in slip and the load at which this shift occurs is given by the Jourasky formula applied to rectangular cross-sections

$$F_0 = \frac{2\,\tau_{slip}\,A}{3} \tag{1}$$

where $A = 4bh$ is the area of the cross-section and $\tau_{slip} = \mu p$ is the maximum shear stress at the interface. The corresponding deflection is obtained by substituting $F_0$ in the formula of a simply supported beam

$$w_0 = \frac{2F_0L^3}{48EI_{p-s}} \tag{2}$$

where $w_0$ is the deflection at the middle of the structure, $F_0$ is the external applied load, E is the Young's modulus of the layers, $I_{p-s}$ is the second moment of area of the pre-slip phase and L is the length of the internal portion of the structure between the supports. During this phase, the second moment of area is maximum and is given by

$$I_{p-s} = \frac{16bh^3}{3} \tag{3}$$

where $h$ and $b$ are the height and the width of a single layer. After the first slip, we assume that the structure behaves as two distinct beams subjected to the same stress state and external loads.

From now on we consider the axial stress distribution as the sum of the axial stress generated by $F_0$, and that of the additional force $F_1$, as shown in Fig. 2a. As explained in detail in our previous work [71], the value of the additional force that causes the second symmetric slip is obtained by computing the static equilibrium of layers 1 and 4 along the longitudinal direction in terms of the axial stresses, which gives

$$F_1 = \frac{F_0}{4} \tag{4}$$

In this case, the evaluation of the corresponding deflection $w_1$ is not trivial. In a typical simply supported beam the overhanging portion of the beam outside the supports does not influence the deformation and therefore is usually neglected. However, in a layer-jamming structure, this condition is no longer true in presence of slip.

Indeed, due to the discontinuity in the shear stress caused by the concentrated load at the support, the structure can be divided in

two regions: an internal region, between the supports, in which the transversal load is constant (V = F/2); an external region, outside the supports, in which the transversal load is zero (V = 0). For this reason, as the external load increases, the portion of the interfaces between the supports will start to slip (when the longitudinal shear stress equals the frictional limit $\mu p$) while the external region will remain cohesive. In reality, sliding propagates also in the external regions (Fig. 5b), although to a lesser extent.

To keep the complexity of the model at an acceptable level, we model the interface between these two adjacent regions as a clamped boundary condition. Under this hypothesis, the additional deflection is given by the Euler–Bernoulli formula for a clamped–clamped beam

$$w_1 = \frac{2F_1 L^3}{192 E I_{pa-s}} \tag{5}$$

During the Partial-slip phase the second moment of area $I_{pa-s}$ decreases by a factor of four and is given by

$$I_{pa-s} = \frac{4bh^3}{3} \tag{6}$$

As the external load exceeds the value of $2(F_0 + F_1)$, all the layers are in slip and the structure enters in the full-slip phase. During this phase the stiffness is minimum and the second moment of area of the structure is given by

$$I_{f-s} = \frac{bh^3}{3} \tag{7}$$

Fig. 2 summarizes the main results of the model: Fig. 2a shows the axial and shear stress distributions inside the structure and Fig. 2b shows a qualitative plot of the relationship between the applied load $F$ and the deflection at the center of the structure $w$. Fig. 2b also shows a graphical representation of the propagation of slip during the three deformation phases.

### 2.2. Jamming structures with an arbitrary number of layers

The model described for a 4-layer-jamming structure can be extended to a more general case with an arbitrary number of layers. As in the previous case, in the initial phase the layers are cohesive and the stiffness is proportional to $(nh)^3$. Then, after the first slip, the stiffness starts to decrease and the behavior becomes nonlinear. In our previous work [71] we demonstrated that slip propagates in an orderly manner from the central to the external interfaces until the last slip, in which all the layers have slipped and the stiffness is proportional to $nh^3$.

Here we report only the general expressions of the additional loads and the corresponding deflections that cause symmetric slips at the $i$th interfaces. For further details please refer to our previous work [71].

$$F_0 = \frac{2\,\mu\, p\, b\, h\, n}{3} \tag{8}$$

$$F_1 = \frac{\mu\, p\, b\, h\, n}{3\,(n-2)} \tag{9}$$

$$F_2 = \frac{2\,\mu\, p\, b\, h\,\left(n^2 - 6\,n + 12\right)}{3\,\left(n^2 - 6\,n + 8\right)} \tag{10}$$

$$F_i = \frac{2\,\mu\, p\, b\, h\,(n^3 - 6\,(i-1)\,n^2 + 12\,(i-1)^2\,n - 8\,(i^3 - 3\,i^2 + 2\,i))}{3\,(n^3 - 6\,(i-1)\,n^2 + (12\,(i-1)^2 - 4)\,n - 8\,(i^3 - 3\,i^2 + 2\,i))}$$
$$i = 3, \ldots, n/2 - 1 \tag{11}$$

$$w_0 = \frac{\mu\, p\, L^3}{3\,\mathrm{E}\, h^2\, n^2} \tag{12}$$

$$w_1 = \frac{\mu\, p\, L^3}{6\,\mathrm{E}\, h^2\, n^2\,(n-2)} \tag{13}$$

$$w_2 = \frac{\mu\, p\, L^3}{6\,\mathrm{E}\, h^2\, n\,\left(n^2 - 6\,n + 8\right)} \tag{14}$$

$$w_i = \frac{\mu\, p\, L^3}{3\,E\, h^2(n^3 - 6\,(i-1)\,n^2 + (12\,(i-1)^2 - 4)\,n - 8\,(i^3 - 3\,i^2 + 2\,i))}$$
$$i = 3, \ldots, n/2 - 1 \tag{15}$$

Notice that only Eqs. (13)–(15) have been modified to take into account the effect of the cohesive external region (clamped boundary condition), as described in the previous subsection.

## 3. Materials and experimental methods

We conducted three-point bending tests to characterize stiffness change in layer-jamming structures, as shown in Fig. 3a. We measured force and central displacement using an MTS Alliance RT/30 electromechanical machine equipped with a 1 kN load cell (MTS-E31665) with 0.01 $N$ resolution. In each test, the distance between the support rollers (1 cm diameter) was set to 10 cm. The specimens were loaded at a constant displacement rate of 5 mm/min until a maximum deflection of 8 mm and then unloaded with the same velocity. Force and deflection data were acquired at a sampling rate of 10 Hz. A vacuum pump (Piab M10A6-BN) connected to a manual vacuum regulator and a highly flexible TPU tube was used to generate the vacuum pressure inside the specimens.

We tested both the influence of the number of layers and vacuum pressure. We fabricated four layer-jamming structures with different numbers of layers (8,12,16,20). Each specimen was tested at a constant vacuum pressure of 68 kPa. We also tested the 20-layer structure at different vacuum pressure levels (24,48,68 kPa). Before each test, specimens were flattened on a rigid planar shelf and then centered on the supports. Each test was repeated three times and mean and standard deviation were computed.

Specimens were fabricated following three main steps. (i) First, sheets of copy paper (Fabriano, Copy2) with height h = 0.1 mm were cut in stripes of 18 × 6 cm. (ii) Then, the envelope was created. A thin film of TPU (0.009 mm thickness) was cut in a rectangle of dimensions 20 × 13 cm. A 3D printed connector was inserted through a tiny hole inside the film and a thin layer of silicone was used to prevent air leakage. (iii) Lastly, sheets were inserted inside the envelope and the edges were sealed through a thermosealer with a welding edge of 2 mm.

In order to compare the experimental results to the theoretical predictions we experimentally evaluated the coefficient of friction $\mu$ = 0.55 and the Young's modulus $E$ = 1.7 GPa. These values are in accordance with the range of values found in literature [73,74]. Due to the difficulties involved in the measure of the Poisson's ratio and the little influence on the analytical predictions, we used a value of $\nu = 0.156$ found in literature [69].

## 4. Numerical simulations

To better understand the validity of our hypothesis, we analyzed the behavior of layer-jamming structures subjected to three-point bending tests using finite element (FE) analyses. All the simulations were conducted using the commercial package Abaqus/Standard 2017 (the Abaqus Python script files are available online as Supporting Information). Due to the symmetry of the problem, only the right half of the structure was simulated. Each layer was modeled as a rectangle with dimensions equal to those of the structure tested in the experiments.

Each layer was discretized using four-node bilinear hybrid plane strain elements with reduced integration (CPE4RH), with a side length equal to half of the layer height. A linear isotropic elastic material with Young's modulus and Poisson's ratio equal to those of the copy paper used in the experiments was assigned to the layers. (E = 1.7 GPa and $\nu = 0.156$). A standard surface-to-surface contact with penalty friction formulation was used to model the interaction between two adjacent layers. A very low value of maximum elastic slip $5 * 10^{-}5$ was set to reduce the undesired non-physical elastic slip.

Vacuum pressure was simulated imposing a uniformly distributed load to all the outer edges of the structure. Symmetric boundary

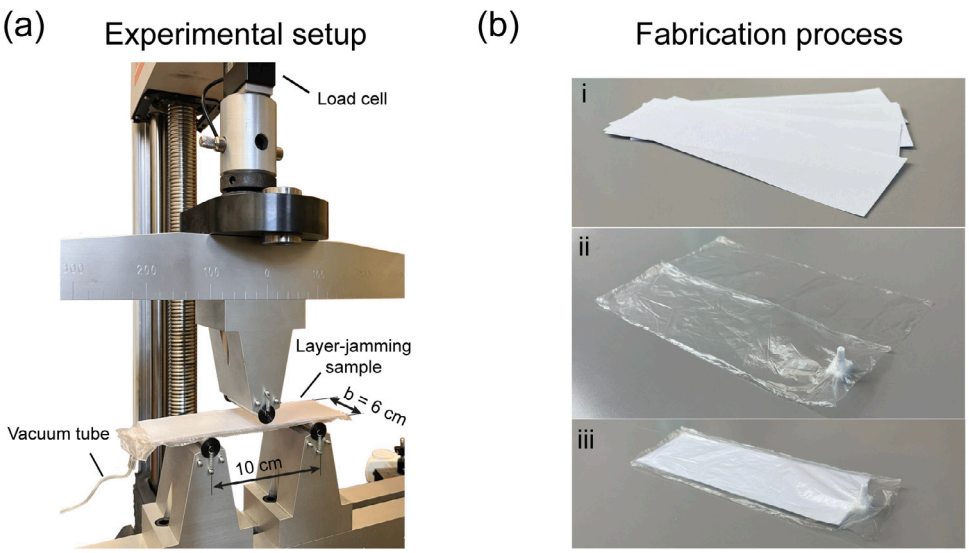


**Fig. 3.** (a) Experimental set-up for the three-point bending tests. (b) Fabrication process of the layer jamming structures. (i) First, sheets of copy paper were cut in stripes. (ii) Then the envelope was created using a thin film of TPU and a 3D printed connector for the vacuum tube. (iii) Lastly, sheets were placed inside the envelope and the edges were sealed with a thermosealer.

conditions were applied on the left edge of each rectangle. The support was simulated by assigning a zero vertical displacement to a node of the bottom layer 50 mm from the center of the structure.

Lastly, the deflection at the center of the structure was simulated by applying a vertical displacement at the first node of the top layer. In all the simulations, nonlinear effects due to large deflections were also taken into account (Nlgeom ON).

## 5. Results

This section reports the results of the three-point bending experiments conducted on layer-jamming structures and the comparison with finite element analysis and the analytical model predictions. The section is organized as follows. We first describe the effect of the number of layers, vacuum pressure and coefficient of friction during loading and unloading tests. Then we discuss the influence of the overhangs and guidelines for design optimization. Notice that for the coefficient of friction no tests were conducted due to the difficulty involved in precisely controlling this parameter experimentally. Therefore, analytical predictions were only compared with finite element simulations.

In all the tests we measured force F and deflection w (Fig. 4a) as described in detail in Section 3. Each combination of parameters was tested three times and mean curves and standard deviation (shaded area in Fig. 4b-e) were computed. Notice that in the analytical model we used the plane-strain Young's modulus $\overline{E} = \frac{E}{1-\nu^2}$ as $b \gg h$.

### 5.1. Number of layers

To study the influence of the number of layers, we tested four structures with different number of layers n (8,12,16,20) with b = 6 cm (width), L = 18 cm (total length), h = 0.1 mm (height of a single layer), E = 1.7 GPa (Young's modulus), $\nu = 0.156$ (Poisson's ratio) and $\mu = 0.55$ (coefficient of friction). The distance between the support was set to 10 cm and a constant vacuum pressure of 68 kPa was applied inside the structures. Tests were conducted following the experimental procedure explained in detail in Section 3.

Fig. 4b shows the comparison between the analytical model, finite element simulations and experiments during the loading phase. As expected, the behavior of these structures is strongly influenced by the number of layers. In particular, both experiments and finite element simulations confirm the assumption that in the first phase (Pre-slip) layer-jamming structures behave like a single linear elastic beam with a bending stiffness that scales with $n^3$, since it is proportional to the second moment of area of the entire structure ($I_{p-s} = b\,n^3 h^3/12$).

In this phase the stiffness is maximum and layers remain cohesive (no slip occurs at the interface between two adjacent layers). As the structure is further deflected, the shear stress increases until it reaches the frictional limit value $\tau_{slip} = \mu p$. at the central interface. The model predicts that this shift will happen when the external load reaches $2F_0$ Eq. (8) which corresponds to a deflection of $w_0$ Eq. (12), and that these values scale with n and $1/n^2$, respectively.

Both experiments and numerical simulations confirmed that the model predict this shift with great accuracy. For example, in the case of 8 layers the model predicts that the structure remains in the pre-slip phase until $w_0 = 11.3$ mm. Indeed, in the range of deflection tested (from 0 to 8 mm), the behavior of the 8-layer structure remains linear. After the first slip the bending stiffness begins to decrease and the behavior becomes nonlinear.

As explained in Section 2, we modeled this behavior using a piecewise linear approximation based on slip propagation. Dots on the model curves indicates the critical load and deflections at which these slip occur and are described by Eqs. (8)–(15). We can observe that as the number of layers increases, the model underestimates the bending stiffness for high deflection with respect to both experiments and numerical simulations. The reason behind this difference is probably due to the increase in the shear stress caused by the increase in the contact pressure generated by the interaction with the supports. This effect is neglected in our model while it is present in finite element simulations.

The loading phase was stopped at a deflection of 8 mm and the energy dissipated by the friction forces, represented by the area under each hysteresis curve, was evaluated by unloading the structures as shown in Fig. 4d. We can observe that the energy loss due to friction increases with the number of layers and that in the unloading phase the system releases the bending energy accumulated in the pre-slip phase. Analytical predictions are in good agreement with experimental results and finite element simulations, demonstrating that the model is also able to accurately capture this hysteretic behavior.

### 5.2. Vacuum pressure

To evaluate the effect of the vacuum pressure we tested the 20-layer jamming structure at three different vacuum pressure levels (24, 48,

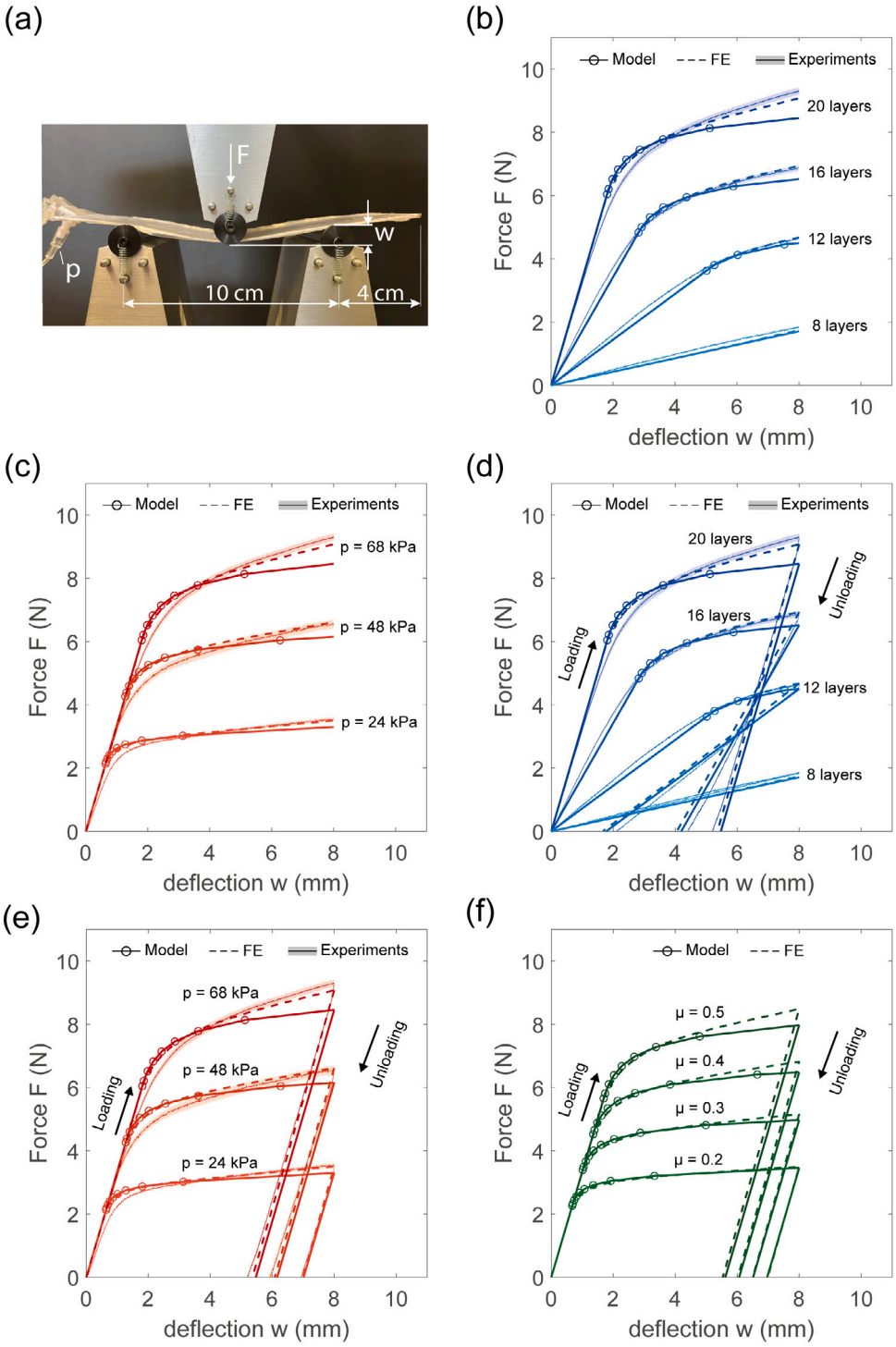


**Fig. 4.** Comparison between theoretical predictions, finite element simulations and experiments. (a) Photograph of the three-point bending set-up used in all the tests. (b) Influence of the number of layers during the loading phase at a constant vacuum pressure (68 kPa). (c) Influence of the vacuum pressure during the loading phase for a 20-layer structure. (d) Energy dissipated by friction during a loading and unloading cycle with a different number of layers. (e) Energy dissipated by friction during a loading and unloading cycle at different vacuum pressure. (f) Energy dissipated by friction during a loading and unloading cycle with different coefficients of friction.

68 kPa). Fig. 4c shows the comparison between the analytical model, finite element simulations and experiments during the loading phase.

The model predicts that the bending stiffness in the initial phase is not influenced by the vacuum pressure and that all the critical loads and deflections scale with the vacuum pressure p, as described by Eqs. (8)–(15). This effect is captured by the model and reflected in both experiments and finite element simulations. We can observe that the model underestimates the bending stiffness for high deflection as the vacuum pressure increases.

As discussed previously the reason behind this difference is probably due to the increase in the contact pressure in correspondence of the supports. Even in this case, the loading phase was stopped at 8 mm and the structures were unloaded (Fig. 4e). Both experiments and finite element simulations confirm that the energy loss due to friction

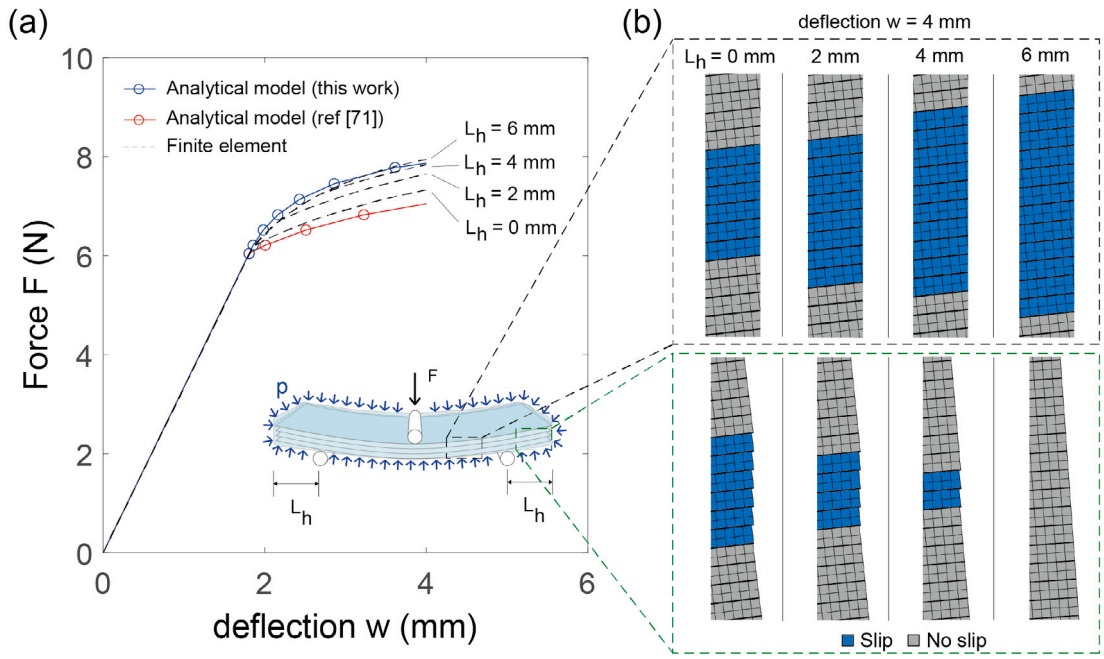


**Fig. 5.** Influence of the length of the overhangs on the bending stiffness of layer jamming structures. (a) Comparison between theoretical predictions and finite element simulations at different overhang lengths $L_h$. (b) Images extracted from finite element simulations at a deflection of w = 4 mm, showing the propagation of slip both in the internal and external regions.

increases almost linearly with the vacuum pressure, as predicted by the model.

### 5.3. Coefficient of friction

As explained previously no tests were conducted to evaluate the influence of the friction coefficient. However, we compared analytical predictions with finite element simulations for a structure with 20 layers with different friction coefficients $\mu$ (0.2, 0.3, 0.4, 0.5). The vacuum pressure was set to 70 kPa and all the dimensions were set equal to the real structure used in the experiments.

As expected, changing either the coefficient of friction or the vacuum pressure has the same influence on the behavior of the structure, as described by Eqs. (8)–(15). Also in this case the energy dissipated by friction scale almost linearly with the coefficient of friction $\mu$.

### 5.4. Influence of the overhangs on the bending stiffness of the structure

For a typical single-layered beam subjected to a 3-point bending test, the curvature maintains a constant sign and the overhangs (regions of the beam outside the supports) do not influence its stiffness. However, for layer jamming structures, experiments and finite elements simulations have shown that the curvature sign changes and the overhangs remain almost flat, resembling the elastica of a clamped–clamped beam.

As described in Section 2, we hypothesize that this counterintuitive behavior can be attributed to the difference in slip propagation between the regions inside and outside the supports. In the internal region (between the supports) the transverse load is constant and equal to (F/2), while outside the support, it is zero. As the transverse load increases, the shear stress at the interfaces between the support increases. Therefore, when the shear stress reaches the frictional limit $\mu p$, the interfaces between the supports begin to slip, while the external regions remain attached.

Based on this assumption, in this work we considered the imaginary vertical line starting from the supports and separating the internal and the external regions as perfectly clamped after the first slip. To test the validity of our hypothesis we conducted finite elements simulations at different values of the overhanging length $L_h$ for a structure with 20 layers subjected to a vacuum pressure p = 68 kPa and with all the other parameters equal to the real structures used in the experiments.

Fig. 5a shows the comparison between the analytical model described in this work, the analytical model presented in [71] (which neglects the overhangs) and finite element simulations at different overhang lengths $L_h$. In the first phase (Pre-slip), finite element simulations are in excellent agreement with the analytical models, confirming that when no slips occur, the presence of the overhangs has no effect on the bending stiffness of the structure.

In this initial phase, the structure behaves like a single-layered beam, since both the internal and external interfaces remain cohesive. However, after the first slip, finite element simulations show that the bending stiffness is minimum for $L_h = 0$ and then increases with $L_h$ until it converges to a maximum value as depicted in Fig. 5a. Interestingly, it is worth noting that all the possible behaviors obtained by varying $L_h$ fall between an upper and a lower limit that are well represented by the analytical model proposed in this work (perfectly clamped) and the previously published model [71] (simply supported).

Another important aspect is highlighted in Fig. 5b. Here we show images extracted from finite element simulations at the maximum deflection w = 4 mm, both at the free end of the external region (green dashed box) and at an internal region between the supports (black dashed box), for different values of $L_h$. Images show that the propagation of slip in the internal region follows an opposite trend with respect to the external region. In particular, as $L_h$ increases the number of interfaces that are in slip decrease at the free end while increase in the internal region.

This fundamental aspect is also captured by the model (blue dots greater than red dots) and can be easily explained by considering that the bending stiffness grows with the increase in $L_h$. Having a higher bending stiffness means that the transverse load required to obtain the same deflection will be greater. Thus, higher transverse loads lead to higher shear stress at the interfaces, resulting in more interfaces that reach the frictional limit in the internal region.

Finally, Fig. 6 shows the comparison between the theoretical models and finite elements simulations at different number of layers, vacuum

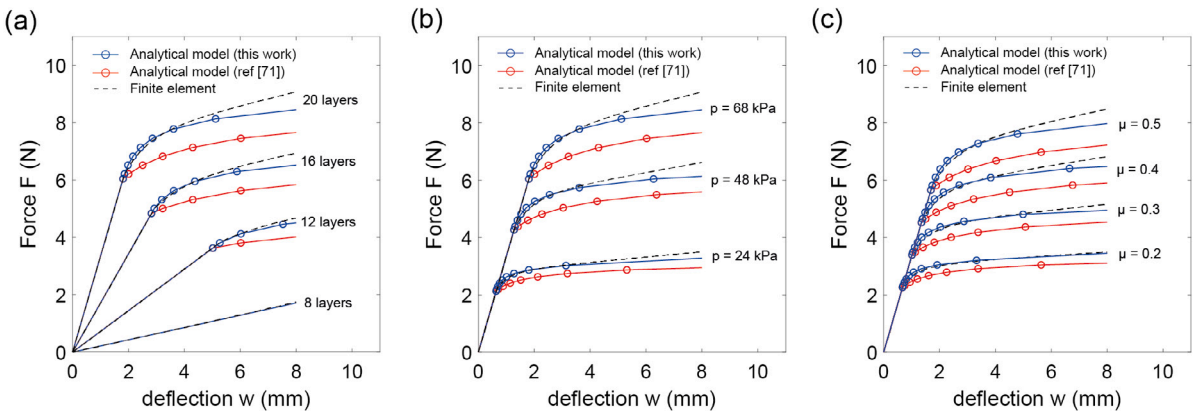


**Fig. 6.** Comparison between the model presented in this work, the analytical model of [71] and finite element simulations, varying the number of layers (a) vacuum pressure (b) and coefficient of friction (c).

pressure and coefficient of friction. All the dimensions, material properties and boundary conditions were chosen equal to those used in the experiments reported previously.

As already explained, all the plots show that until reaching the first slip, both models and finite elements simulations are in perfect agreement. Then, after the first slip, the model proposed in [71] underestimates the bending stiffness of the structure while the model presented in this work remains in very good agreement with finite element results, confirming the importance of introducing the stiffness increase caused by the overhangs in the analytical formulation.

### 5.5. Design optimization

Now that we have experimentally verified the accuracy of our analytical model across a range of conditions, our focus shifts to identifying performance characteristics and trends that can provide insights for designing and optimizing layer jamming structures for real-world applications. For example, consider an application in which we want to maximize the stiffness ratio between the jammed and unjammed states (e.g. for a soft ankle foot orthosis).

The goal is to design a system that is as soft as possible in its rest state (to ensure comfort) and as rigid as possible upon activation (to prevent ankle sprains). To achieve this goal we need to design a structure with as many layers as possible within the maximum allowable total thickness. As described previously, the stiffness ratio between the jammed and unjammed state scales with the square of the number of layers ($n^2$), thus decreasing the thickness of the layers leads to an increase in the number of layers and consequently an increase in the stiffness ratio.

For example, with a structure of 100 layers with a thickness of 0.1 mm (total thickness 1 cm), we would obtain an increase in stiffness of 4 order magnitude. However, if the structure is subjected to high external loads or deflections (e.g. unexpected fall) the layers will enter in slip and the stiffness will dramatically decrease. This problem could be mitigated by increasing either the vacuum pressure or the coefficient of friction, which has the effect of increasing the loads and deflections at which the structure will enter in slip, as shown in Fig. 4c and 4.f.

Similarly, the vacuum pressure and the coefficient of friction play an important role also in applications in which we want to tune the dynamic response of the systems (e.g. soft dampers, hand tremor suppressors). As shown in Fig. 4e–f, the energy dissipated by friction scales almost linearly with both the vacuum pressure and the coefficient of friction. Therefore, if we want to double the energy dissipated by the system, then we can double either the vacuum pressure or the coefficient of friction. The vacuum pressure can be adjusted on command by a vacuum regulator, thus the damping tuning can also be controlled in real-time.

## 6. Conclusions

We presented a novel theoretical approach that predicts the complex nonlinear behavior of multilayer-jamming structures beyond the initial deformation phase. We extended our previously published analytical model [71] introducing the increase in stiffness caused by the overhangs outside the supports. The experimental validation of the proposed approach was discussed by performing three-point bending tests, which showed good agreement between the predicted and actual behavior, especially considering that no fitting coefficients were adopted. Highly accurate finite element models were also constructed to further validate the theoretical predictions, showing how slip propagates between the layers.

Experimental and numerical evidence confirmed all the most important prediction of the model. Specifically, the model shows that the nonlinear behavior, beyond the initial deformation phase, can be well described with a piecewise linear approximation between subsequent slips. The stiffness declines as the slip propagates inside the structure. In particular, the model predicts that slip starts at the innermost interface and then progressively propagates toward the outer interfaces.

We also discovered that the bending stiffness increases with the length of the overhangs outside the supports, until it converges to a maximum value, which is well approximated by our theoretical predictions. Our model also provides a rapid design tool for the fabrication of improved layer jamming structure, predicting the influence of the main design parameters (number of layers, vacuum pressure and coefficient of friction) as well as the energy dissipated by friction during a load–unload cycle. We found that the energy dissipated by friction in a load–unload cycle scales almost linearly with both the vacuum pressure and the coefficient of friction.

We believe that this work represents a significant step forward in understanding the complex intrinsic mechanics of layer-jamming structures that will help researchers to design more advanced variable stiffness applications in soft robotics.

## CRediT authorship contribution statement

**Fabio Caruso:** Conceptualization, Software, Validation, Investigation, Data curation, Writing – original draft, Writing – review & editing, Visualization. **Giacomo Mantriota:** Conceptualization, Methodology, Validation, Writing – review & editing, Supervision. **Vincenzo Moramarco:** Software, Validation, Investigation, Writing – review & editing. **Giulio Reina:** Conceptualization, Methodology, Validation, Writing – review & editing, Supervision.

## Declaration of competing interest

The authors declare that they have no known competing financial interests or personal relationships that could have appeared to influence the work reported in this paper.

## Data availability

Data will be made available on request

## Appendix A. Supplementary data

Supplementary material related to this article can be found online at https://doi.org/10.1016/j.ijmecsci.2023.108325.

## References


[1] Whitesides GM. Soft robotics. Angew Chem, Int Ed Engl 2018;57(16):4258–73.
[2] Majidi C. Soft-matter engineering for soft robotics. Adv Mater Technol 2019;4(2):1800477.
[3] Cianchetti M, Laschi C, Menciassi A, Dario P. Biomedical applications of soft robotics. Nat Rev Mater 2018;3(6):143–53.
[4] Polygerinos P, Correll N, Morin SA, Mosadegh B, Onal CD, Petersen K, et al. Soft robotics: Review of fluid-driven intrinsically soft devices; manufacturing, sensing, control, and applications in human-robot interaction. Adv Energy Mater 2017;19(12):1700016.
[5] Rus D, Tolley MT. Design, fabrication and control of soft robots. Nature 2015;521(7553):467–75.
[6] Lee C, Kim M, Kim YJ, Hong N, Ryu S, Kim HJ, et al. Soft robot review. Int J Control Autom Syst 2017;15:3–15.
[7] Laschi C, Mazzolai B, Cianchetti M. Soft robotics: Technologies and systems pushing the boundaries of robot abilities. Science Robotics 2016;1(1):eaah3690.
[8] Wang H, Totaro M, Beccai L. Toward perceptive soft robots: Progress and challenges. Adv Sci 2018;5(9):1800541.
[9] Rich SI, Wood RJ, Majidi C. Untethered soft robotics. Nat Electron 2018;1(2):102–12.
[10] Manti M, Cacucciolo V, Cianchetti M. Stiffening in soft robotics: A review of the state of the art. IEEE Robot Autom Mag 2016;23(3):93–106.
[11] Wang L, Yang Y, Chen Y, Majidi C, Iida F, Askounis E, et al. Controllable and reversible tuning of material rigidity for robot applications. Mater Today 2018;21(5):563–76.
[12] Yang Y, Li Y, Chen Y. Principles and methods for stiffness modulation in soft robot design and development. Bio-Design Manuf 2018;1(1):14–25.
[13] Blanc L, Delchambre A, Lambert P. Flexible medical devices: Review of controllable stiffness solutions. In: Actuators. Vol. 6, (3):MDPI; 2017, p. 23.
[14] Runciman M, Darzi A, Mylonas GP. Soft robotics in minimally invasive surgery. Soft Robot 2019;6(4):423–43.
[15] Cianchetti M, Ranzani T, Gerboni G, Nanayakkara T, Althoefer K, Dasgupta P, Menciassi A. Soft robotics technologies to address shortcomings in today's minimally invasive surgery: the STIFF-FLOP approach. Soft Robot 2014;1(2):122–31.
[16] Yin J, Hinchet R, Shea H, Majidi C. Wearable soft technologies for haptic sensing and feedback. Adv Funct Mater 2021;31(39):2007428.
[17] Salazar SV, Pacchierotti C, de Tinguy X, Maciel A, Marchal M. Altering the stiffness, friction, and shape perception of tangible objects in virtual reality using wearable haptics. IEEE Trans Haptics 2020;13(1):167–74.
[18] Shintake J, Cacucciolo V, Floreano D, Shea H. Soft robotic grippers. Adv Mater 2018;30(29):1707035.
[19] Wei Y, Chen Y, Ren T, Chen Q, Yan C, Yang Y, et al. A novel, variable stiffness robotic gripper based on integrated soft actuating and particle jamming. Soft Robot 2016;3(3):134–43.
[20] Wang W, Ahn S-H. Shape memory alloy-based soft gripper with variable stiffness for compliant and effective grasping. Soft Robot 2017;4(4):379–89.
[21] Zhong G, Hou Y, Dou W. A soft pneumatic dexterous gripper with convertible grasping modes. Int J Mech Sci 2019;153:445–56.
[22] Wang Y, Li L, Hofmann D, Andrade JE, Daraio C. Structured fabrics with tunable mechanical properties. Nature 2021;596(7871):238–43.
[23] Kwon J, Choi I, Park M, Moon J, Jeong B, Pathak P, et al. Selectively stiffening garments enabled by cellular composites. Adv Mater Technol 2022;2101543.
[24] Shah DS, Yang EJ, Yuen MC, Huang EC, Kramer-Bottiglio R. Jamming skins that control system rigidity from the surface. Adv Funct Mater 2021;31(1):2006915.
[25] Tonazzini A, Mintchev S, Schubert B, Mazzolai B, Shintake J, Floreano D. Variable stiffness fiber with self-healing capability. Adv Mater 2016;28(46):10142–8.
[26] Baniasadi M, Foyouzat A, Baghani M. Multiple shape memory effect for smart helical springs with variable stiffness over time and temperature. Int J Mech Sci 2020;182:105742.
[27] De Vicente J, Klingenberg DJ, Hidalgo-Alvarez R. Magnetorheological fluids: a review. Soft Matter 2011;7(8):3701–10.
[28] Wang T, Zhang J, Li Y, Hong J, Wang MY. Electrostatic layer jamming variable stiffness for soft robotics. IEEE/ASME Trans Mechatronics 2019;24(2):424–33.
[29] Fitzgerald SG, Delaney GW, Howard D. A review of jamming actuation in soft robotics. In: Actuators. Vol. 9, (4):MDPI; 2020, p. 104.
[30] Hauser S, Robertson M, Ijspeert A, Paik J. Jammjoint: A variable stiffness device based on granular jamming for wearable joint support. IEEE Robot Autom Lett 2017;2(2):849–55.
[31] Jaeger HM. Celebrating soft matter's 10th anniversary: Toward jamming by design. Soft Matter 2015;11(1):12–27.
[32] Yang B, Baines R, Shah D, Patiballa S, Thomas E, Venkadesan M, et al. Reprogrammable soft actuation and shape-shifting via tensile jamming. Sci Adv 2021;7(40):eabh2073.
[33] Jadhav S, Majit MRA, Shih B, Schulze JP, Tolley MT. Variable stiffness devices using fiber jamming for application in soft robotics and wearable haptics. Soft Robot 2022;9(1):173–86.
[34] Brancadoro M, Manti M, Tognarelli S, Cianchetti M. Fiber jamming transition as a stiffening mechanism for soft robotics. Soft Robot 2020;7(6):663–74.
[35] Pinskier J, Brett J, Hanson L, Surdo KL, Howard D. Jammkle: Fibre jamming 3D printed multi-material tendons and their application in a robotic ankle. In: 2022 IEEE/RSJ international conference on intelligent robots and systems. IROS, IEEE; 2022, p. 8507–14.
[36] Choi WH, Kim S, Lee D, Shin D. Soft, multi-DoF, variable stiffness mechanism using layer jamming for wearable robots. IEEE Robot Autom Lett 2019;4(3):2539–46.
[37] Lin Y, Yang G, Liang Y, Zhang C, Wang W, Qian D, et al. Controllable stiffness origami "skeletons" for lightweight and multifunctional artificial muscles. Adv Funct Mater 2020;30(31):2000349.
[38] Brown E, Rodenberg N, Amend J, Mozeika A, Steltz E, Zakin MR, et al. Universal robotic gripper based on the jamming of granular material. Proc Natl Acad Sci 2010;107(44):18809–14.
[39] Amend JR, Brown E, Rodenberg N, Jaeger HM, Lipson H. A positive pressure universal gripper based on the jamming of granular material. IEEE Trans Robot 2012;28(2):341–50.
[40] Licht S, Collins E, Mendes ML, Baxter C. Stronger at depth: Jamming grippers as deep sea sampling tools. Soft Robot 2017;4(4):305–16.
[41] Ranzani T, Gerboni G, Cianchetti M, Menciassi A. A bioinspired soft manipulator for minimally invasive surgery. Bioinspiration Biomim 2015;10(3):035008.
[42] Cavallo A, Brancadoro M, Tognarelli S, Menciassi A. A soft retraction system for surgery based on ferromagnetic materials and granular jamming. Soft Robot 2019;6(2):161–73.
[43] Henann DL, Kamrin K. Continuum modeling of secondary rheology in dense granular materials. Phys Rev Lett 2014;113(17):178001.
[44] Henann DL, Kamrin K. A predictive, size-dependent continuum model for dense granular flows. Proc Natl Acad Sci 2013;110(17):6730–5.
[45] Blanc L, François B, Delchambre A, Lambert P. Characterization and modeling of granular jamming: models for mechanical design. Granul Matter 2021;23:1–13.
[46] Kumar R, Rommel S, Jauffrès D, Lhuissier P, Martin CL. Effect of packing characteristics on the discrete element simulation of elasticity and buckling. Int J Mech Sci 2016;110:14–21.
[47] Li L, Marteau E, Andrade JE. Capturing the inter-particle force distribution in granular material using LS-DEM. Granul Matter 2019;21:1–16.
[48] Behringer RP, Chakraborty B. The physics of jamming for granular materials: a review. Rep Progr Phys 2018;82(1):012601.
[49] Baule A, Morone F, Herrmann HJ, Makse HA. Edwards statistical mechanics for jammed granular matter. Rev Modern Phys 2018;90(1):015006.
[50] Aktaş B, Narang YS, Vasios N, Bertoldi K, Howe RD. A modeling framework for jamming structures. Adv Funct Mater 2021;31(16):2007554.
[51] Kim Y-J, Cheng S, Kim S, Iagnemma K. A novel layer jamming mechanism with tunable stiffness capability for minimally invasive surgery. IEEE Trans Robot 2013;29(4):1031–42.
[52] Kim Y-J, Cheng S, Kim S, Iagnemma K. Design of a tubular snake-like manipulator with stiffening capability by layer jamming. In: 2012 IEEE/RSJ international conference on intelligent robots and systems. IEEE; 2012, p. 4251–6.
[53] Ou J, Yao L, Tauber D, Steimle J, Niiyama R, Ishii H. Jamsheets: thin interfaces with tunable stiffness enabled by layer jamming. In: Proceedings of the 8th international conference on tangible, embedded and embodied interaction. 2014, p. 65–72.
[54] Yang Y, Zhang Y, Kan Z, Zeng J, Wang MY. Hybrid jamming for bioinspired soft robotic fingers. Soft Robot 2020;7(3):292–308.
[55] Fang B, Sun F, Wu L, Liu F, Wang X, Huang H, et al. Multimode grasping soft gripper achieved by layer jamming structure and tendon-driven mechanism. Soft Robot 2022;9(2):233–49.
[56] Wang X, Wu L, Fang B, Xu X, Huang H, Sun F. Layer jamming-based soft robotic hand with variable stiffness for compliant and effective grasping. Cognitive Computation Syst 2020;2(2):44–9.
[57] Gerez L, Gao G, Liarokapis M. Laminar jamming flexure joints for the development of variable stiffness robot grippers and hands. In: 2020 IEEE/RSJ international conference on intelligent robots and systems. IROS, IEEE; 2020, p. 8709–15.
[58] Gerez L, Gao G, Dwivedi A, Liarokapis M. A hybrid, wearable exoskeleton glove equipped with variable stiffness joints, abduction capabilities, and a telescopic thumb. Ieee Access 2020;8:173345–58.
[59] Dezaki ML, Bodaghi M. Shape memory meta-laminar jamming actuators by 4D printing. Soft Matter 2023.

[60] Aktaş B, Howe RD. Flexure mechanisms with variable stiffness and damping using layer jamming. In: 2019 IEEE/RSJ international conference on intelligent robots and systems. IROS, IEEE; 2019, p. 7616–21.
[61] Ibrahimi M, Paternò L, Ricotti L, Menciassi A. A layer jamming actuator for tunable stiffness and shape-changing devices. Soft Robot 2021;8(1):85–96.
[62] Narang YS, Aktaş B, Ornellas S, Vlassak JJ, Howe RD. Lightweight highly tunable jamming-based composites. Soft Robot 2020;7(6):724–35.
[63] Choi I, Corson N, Peiros L, Hawkes EW, Keller S, Follmer S. A soft, controllable, high force density linear brake utilizing layer jamming. IEEE Robot Autom Lett 2017;3(1):450–7.
[64] Narang YS, Degirmenci A, Vlassak JJ, Howe RD. Transforming the dynamic response of robotic structures and systems through laminar jamming. IEEE Robot Autom Lett 2017;3(2):688–95.
[65] Wanasinghe A, Awantha W, Kavindya A, Kulasekera A, Chathuranga D, Senanayake B. A layer jamming soft glove for hand tremor suppression. IEEE Trans Neural Syst Rehabil Eng 2021;29:2684–94.
[66] Sayyad AS, Ghugal YM. Bending, buckling and free vibration of laminated composite and sandwich beams: A critical review of literature. Compos Struct 2017;171:486–504.
[67] Sahoo R, Singh B. A new shear deformation theory for the static analysis of laminated composite and sandwich plates. Int J Mech Sci 2013;75:324–36.
[68] Hajianmaleki M, Qatu MS. Vibrations of straight and curved composite beams: A review. Compos Struct 2013;100:218–32.
[69] Narang YS, Vlassak JJ, Howe RD. Mechanically versatile soft machines through laminar jamming. Adv Funct Mater 2018;28(17):1707136.
[70] Vasios N, Narang Y, Aktaş B, Howe R, Bertoldi K. Numerical analysis of periodic laminar and fibrous media undergoing a jamming transition. Eur J Mech A Solids 2019;75:322–9.
[71] Caruso F, Mantriota G, Afferrante L, Reina G. A theoretical model for multi-layer jamming systems. Mech Mach Theory 2022;172:104788.
[72] Caruso F, Mantriota G, Reina G. An analytical model for cantilever layer-jamming structures. In: The international conference of IFToMM ITALY. Springer; 2022, p. 193–200.
[73] Johansson A. Paper friction-influence of measurement conditions. Tappi J 1998;81:175.
[74] Yoshihara H, Yoshinobu M. Effects of specimen configuration and measurement method of strain on the characterization of tensile properties of paper. J Wood Sci 2014;60(4):287–93.